Construction and Building Materials 98 (2015) 397–406

Contents lists available at ScienceDirect

Construction and Building Materials

journal homepage: www.elsevier.com/locate/conbuildmat

Characterization of alkali activated slag–fly ash blends containing nano-silica

X. Gao, Q.L. Yu *, H.J.H. Brouwers

Department of the Built Environment, Eindhoven University of Technology, P.O. Box 513, 5600 MB Eindhoven, The Netherlands

HIGHLIGHTS

- The nano-silica addition reduces the flowability and slightly retards the early age reaction.
- The gel structure remains stable regardless of nano-silica content and slag/fly ash ratio.
- The addition of nano-silica slightly increases the chemically bound water content.
- A nano-silica content of around 2% presents the optimum strength and porosity.

ARTICLE INFO

Article history:
Received 9 May 2015
Received in revised form 1 August 2015
Accepted 9 August 2015

Keywords:
Alkali activation
Fresh behavior
Slag–fly ash blends
Nano-silica
Reaction kinetics
Porosity
Compressive strength

ABSTRACT

Applying nano-technology/modifications in construction and building materials has shown inspiring results. This paper investigates the effects of nano-silica incorporation on an eco-friendly alkali activated slag–fly ash blends. The fresh behaviors, reaction kinetics, gel structure, porosity and strength of samples with different nano-silica contents and slag/fly ash ratios are analyzed. The results indicate that as the nano-silica content increases, the slump flow is significantly reduced, and the reaction process is slightly retarded according to the setting time and isothermal calorimetry results. The microstructure analysis carried out by FTIR and TG/DSC shows that the addition of nano-silica slightly increases the chemically bound water content. The main reaction product is a chain structured C-A-S-H type gel, regardless of the slag/fly ash ratio and nano-silica content. Increasing the nano-silica content up to around 2% benefits the compressive strength and contributes to a reduced porosity, but further higher nano-silica contents show a negative effect on the strength and the pore refinement becomes less significant. It is suggested that the nano-silica benefits the microstructure and strength by providing additional reactive silica source and the filler effect. Furthermore, the slag content exhibits a dominant role on setting times, early age reaction, compressive strength and porosity in this blended alkali system.

1. Introduction

In order to reduce the negative environmental impacts of cement industry, great attention has been paid to apply alkali activated materials as alternatives to Portland cement. This type of material generally exhibits superior mechanical properties [1], durability [2,3], thermal resistance [4] together with significantly reduced energy costs and carbon emissions [5,6]. Based on the chemical composition of the raw materials, two types of binding systems can be classified: one is the alkali activated slag (Si + Ca) system, having a C-A-S-H type gel with a low Ca/Si ratio and a high Al incorporation as the main reaction product [7]; the other is the alkali activated class F fly ash/metakaolin (Si + Al) system, having N–A–S–H type gels with three-dimensional network as the major reaction products [8]. Both systems exhibit distinct behaviors regarding alkaline and curing demands, setting and hardening processes, strength development due to their differences in reaction mechanism and gel characteristics.

Recently, growing interests have been focused on the blended alkaline system (Na_2O–CaO–Al_2O_3–SiO_2 system) that is prepared by mixing calcium enriched precursors and low calcium aluminosilicates. Compared to either of the individual system, the blended system shows a better control of setting times [9], as well as modified workability [10], shrinkage [11], mechanical properties and durability [12]. Micro-scale analysis reveals that the reaction products are stably coexisting C-(A)-S-H and N-A-S-H type gels with higher degree of cross-linking [13–15], indicating a desirable formation of gel structure. Furthermore, the effects of activator type and dosage, raw materials' composition and curing conditions

* Corresponding author.
E-mail address: q.yu@bwk.tue.nl (Q.L. Yu).

http://dx.doi.org/10.1016/j.conbuildmat.2015.08.086
0950-0618/

on reaction kinetics, gel characters, mechanical properties and durability issues were also intensively investigated [16–21]. The recent progresses in understanding the blended system provide solid basis for further investigations and those modified properties demonstrate a promising future for the application of alkali activated materials.

On the other hand, nano-silica (NS) has recently been utilized in Portland cement based systems as an effective pozzolanic binder for the improvement of mechanical properties and microstructure [22]. Due to its considerably fine particle size, nano-silica has been observed to accelerate the hydration process at early ages [23], refine the pore structure [24,25] and enhance the mechanical properties even at small levels of replacement [26]. Moreover, nano-silica also exhibits ideal pozzolanic activity owing to its amorphous nature and high specific surface area [27,28], which leads to the formation of additional C-S-H gel by reacting with calcium hydroxide and results in a denser matrix [29–31]. Meanwhile, attention has also been paid to apply nano-silica in alkali activated systems. Tanakorn et al. [32] studied the effect of nano-silica on fly ash based geopolymers, showing that increasing the nano-silica content results in the decrease of setting time and the increment of mechanical properties. Microstructure analysis revealed that a nano-silica content up to 2% increases the reaction product and densifies the matrix, but higher nano-silica contents show negative effects. Gao et al. [33] applied nano-silica up to 3% by mass in metakaolin based geopolymers, increased reaction products due to nano-silica addition were observed and an optimum nano-silica content of 1% in terms of strength and porosity was reported. Adak et al. [34] investigated the effect of nano-silica on strength and durability of fly ash based geopolymers, the used nano-silica content was up to 10% by mass. The results showed that a nano-silica content of 6% exhibits appreciable mechanical properties under ambient temperature, as well as less water absorption and reduced charge passed in rapid chloride ion penetration test. As can be noticed, the previous studies showed the superiority of applying nano-silica in alkali activated low calcium systems. However, there are limited mechanism studies and performance evaluations concerning the effect of nano-silica on the blended alkaline system (Na_2O–CaO–Al_2O_3–SiO_2).

The purpose of this study is to understand the influence of nano-silica on fresh behavior, early age reaction kinetics, mechanical properties, reaction products and microstructure of alkali activated slag–fly ash blends. The flowability, setting times, porosity and compressive strength of alkali activated slag–fly ash blends with nano-silica addition are identified. Furthermore, micro-scale analyses are carried out by using isothermal calorimetry, thermogravimetry/differential scanning calorimetry (TG/DSC) and Fourier transform infrared spectroscopy (FTIR).

2. Experiment

2.1. Materials

The solid precursors used in this study were ground granulated blast furnace slag (GGBS, provided by ENCI B.V., the Netherlands) and a commercial Class F fly ash. Their major chemical compositions were analyzed by X-ray fluorescence and are shown in Table 1. The detailed particle size distributions of solid raw materials and nano-silica, measured applying a light scattering technique using Mastersizer 2000, are given in Fig. 1. The used slag has a median particle size (d_{50}) of 12.43 μm and a specific density of 2.93 g/cm^3; while the fly ash has a d_{50} of 22.06 μm and a specific density of 2.30 g/cm^3. A commercially available nano-silica slurry is selected, the slurry has a solid content of 50 wt.%, a d50 of 0.12 μm and a density of 1.4 g/cm^3. The chemical composition of nano-silica provided by the supplier is listed in Table 1. Concerning the alkaline activators, commercial sodium silicate solution (27.69% SiO_2, 8.39% Na_2O and 63.92% H_2O by mass) and analytical level of sodium hydroxide pellets (99 wt.%) were used. The desired activator modulus (Ms, SiO_2/Na_2O molar ratio) was achieved by adding the appropriate amount of sodium hydroxide pellets into the sodium silicate solution. Distilled water was added in order to reach the desired water/binder ratio. The mixed activator solution was cooled down to room temperature prior to further use.

Table 1
Major chemical composition of slag, fly ash and nano-silica.

Oxides (wt.%)	Fly ash	Slag	Nano-silica
SiO_2	54.62	34.44	98.68
Al_2O_3	24.42	13.31	0.37
CaO	4.44	37.42	0.09
MgO	1.43	9.89	–
Fe_2O_3	7.21	0.47	–
Na_2O	0.73	0.34	0.32
K_2O	1.75	0.47	0.35
SO_3	0.46	1.23	–
LOI	2.80	1.65	–

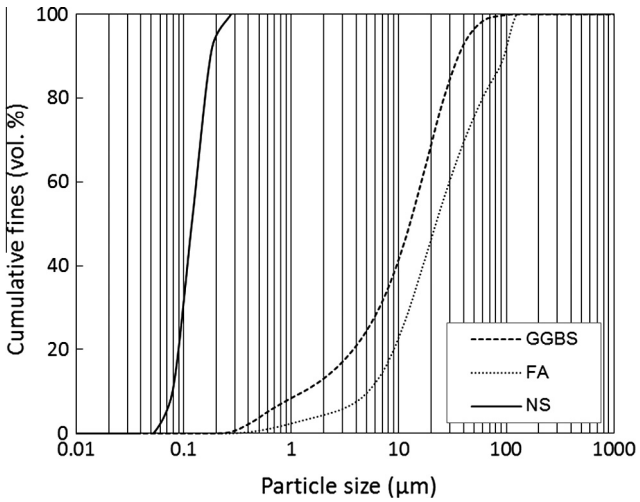

Fig. 1. Particle size distributions of raw materials.

2.2. Sample preparation

The activator used in this study has an equivalent sodium oxide (Na_2O) content of 5% by mass of the binder and an activator modulus of 1.4 for all mixes. The target activator modulus was reached by mixing sodium silicate solution and sodium hydroxide pellets with a solution/pellets mass ratio of 6.41. The water/binder ratio was kept constant at 0.35 in all mixtures. The water consisted of the added distilled water, the water contained in the activator solution and nano-silica slurry. The chosen Na_2O content and water/binder ratio were preliminarily determined that would provide sufficient alkalinity without efflorescence and satisfying flowability, respectively [21,35]. The slag/fly ash ratios of 70/30 and 30/70 by mass and nano-silica replacement from 0% to 3% by mass were used. The detailed information of mix proportions is listed in Table 2. The paste samples were prepared in a laboratory mixer; firstly the solid raw materials were added into the mixer and mixed for 1 min, followed by the nano-silica slurry and the activating solution; then their mixtures were mixed at a slow speed for 30 s and rested for 30 s before another 120 s at a medium speed. The fresh paste/mortar was poured into plastic molds of 40 × 40 × 160 mm^3 and vibrated for 1 min, then covered with a plastic film on the top surface for 24 h; finally all specimens were demolded and cured at a temperature of 20 °C and a relative humidity of 95% until the testing age.

2.3. Testing methods

The workability of paste samples were tested by the mini spread-flow test applying the Hägermann cone according to EN 1015-3 [36]. Fresh samples were transferred into a standard conical ring and a free flow without jolting was allowed. Two diameters that are perpendicular to each other were determined and the mean value was recorded as the slump flow. The initial and final setting times were measured by a Vicat needle method as described in EN 196-3 [37]. The determined values were an average of three samples.

The reaction kinetics was investigated by an isothermal calorimeter (TAM Air, Thermometric). Solid raw materials were firstly mixed with activating solution externally for around 1 min vibrated by an electrical vibrator, then the mixed paste was injected into the ampoule and sealed by a lid, and loaded into the calorimeter. All measurements were conducted for 72 h under a constant temperature of 20 °C.

Table 2
Mix proportions of alkali activated slag–fly ash blends with nano-silica addition.

Mixture	Activator	Solid raw materials (wt.%)			w/b
		Slag	Fly ash	Nano-silica	
A730	Na_2O:5%; Ms:1.4	70	30	0	0.35
A370		30	70		
A731		69.3	29.7	1	
A371		29.7	63.9		
A732		68.6	29.4	2	
A372		29.4	68.6		
A733		67.9	29.1	3	
A373		29.1	67.9		

Fourier transform infrared spectroscopy (FTIR) measurement was performed to the samples at the age of 28 days in a Varian 3100 instrument with the wavenumbers ranging from 4000 to 600 cm^{-1} at a resolution of 1 cm^{-1}. The thermogravimetric and differential scanning calorimeter (TG/DSC) analyses were conducted by using a STA 449 F1 instrument, and ground powder samples after 28 days of curing were heated up to 1000 °C at a rate of 5 °C/min with nitrogen as the carrier gas. The temperature was held isothermally at 105 °C for 2 h during the heating process.

The compressive strength tests were carried out according to EN 196-1 [38]. $40 \times 40 \times 40$ mm^3 cubes were prepared and tested at the ages of 3, 7 and 28 days respectively, and the compressive strength value for each sample was obtained from the average of six specimens. The porosity was measured by applying the vacuum-saturation technique following the description given in NT Build 492 [39]. The water permeable porosity is calculated as:

$$P\ (\%) = \frac{Ms - Md}{Ms - Mw} \times 100\% \quad (1)$$

where P (%) is the water permeable porosity, Ms (g) refers to the mass of the saturated sample in surface-dry condition in air, Mw (g) is the mass of water-saturated sample in water and Md (g) is the mass of oven dried sample.

3. Results and discussion

3.1. Flowability and setting times

The slump flows of the fresh alkali activated slag–fly ash pastes with nano-silica replacements from 0% to 3% are depicted in Fig. 2. The figure briefly presents the relations between the slag/fly ash ratio, nano-silica content and the workability of blended pastes. It can be seen that with a constant nano-silica content, a lower slag/fly ash ratio exhibits a better workability. For instance, in samples without nano-silica addition, when the slag/fly ash ratio changes from 70/30 to 30/70, the slump flow increases from 30.7 to 32.4 cm; similar results are also found in mixes with the nano-silica replacements. This phenomenon is in agreement with previous studies that a lower slag to fly ash ratio exhibits a better flowability in their blends, which can be explained by the morphology differences between slag and fly ash, as slag shows a higher water demand than fly ash due to its angular particle shape and larger surface area [40,41]. On the other hand, compared to the effect of slag/fly ash ratio, the nano-silica content exhibits a more prominent influence on flowability even at small dosages. As shown in Fig. 2, the slump flow dramatically decreases with the increase of nano-silica content: for the samples with a slag/fly ash ratio of 70/30, the slump flow is decreased by 18.2%, 32.2% and 45.9% when the nano-silica content increases from 1% to 2% and 3%, respectively; similarly, decreasing rates of 16.8%, 30.8% and 42.2% are shown in mixtures with a slag/fly ash ratio of 30/70. The remarkable reduction of slump flow could be attributed to the much finer particle size of nano-silica (d50 of 0.12 μm) than slag and fly ash (d50 of 12.43 and 22.06 μm, respectively), therefore an especially larger surface area in total is presented as a result, which leads to a decrease in slump flow. Meanwhile, due to the high reactivity of nano-silica particles that contain unsaturated Si–O bonds, a certain amount of water in the solution can be retained around the nano-silica particles with the formation of Si–OH [42,43]. This process may also contribute to the significant reduction of slump flow by decreasing the total amount of effective mixing water.

Fig. 3 presents the influence of nano-silica and slag/fly ash ratio on the initial and final setting times of alkali activated slag–fly ash blends. It can be seen that for a constant nano-silica content, samples with a lower slag/fly ash ratio exhibit longer initial and final setting times in general. For instance, the sample with a slag/fly ash ratio of 70/30 and without nano-silica shows an initial setting time of 27 min, while this value increases to 76 min in the sample with a slag/fly ash ratio of 30/70; and the final setting time also increases from 71 min to 128 min. The significant influence of slag content on the setting times of alkali activated slag–fly ash blends is also reported in previous studies [16,44,45]. The acceleration effect of slag on setting times is mainly due to its vulnerable amorphous structure that consists of large amount network-modifying cations (especially Ca), which exhibit high reactivity under alkali conditions. Thus a faster reaction process and shorter setting time are shown as a result of the faster dissolution rate of Ca, Si and Al units from slag and higher total amount of dissolved units in the

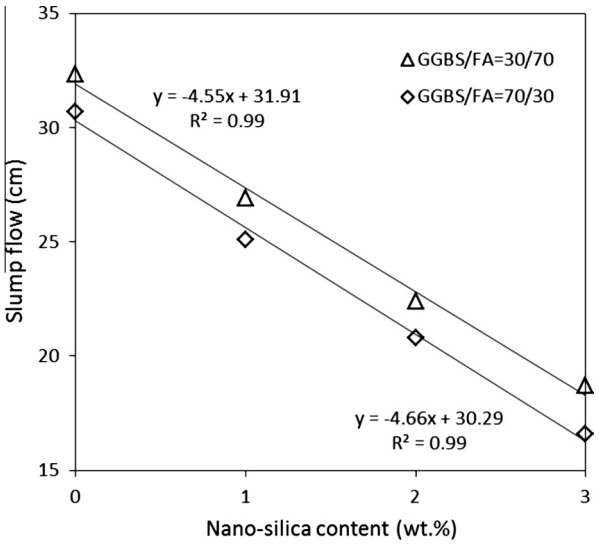

Fig. 2. Slump flow of AA slag–fly ash blends with nano-silica addition.

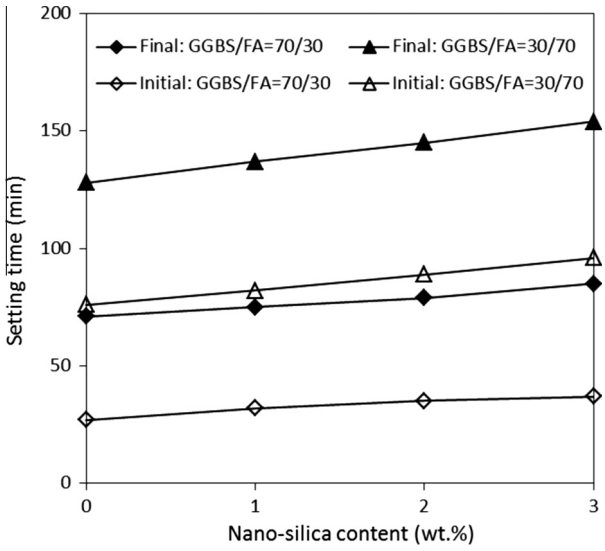

Fig. 3. Setting time of AA slag–fly ash blends with nano-silica addition.

slag–fly ash blends. Concerning the effect of nano-silica, it can be seen that both initial and final setting times are gradually increasing with the increase of nano-silica content, and its effect on setting time is more significant in mixtures with a lower slag/fly ash ratio. Specifically, the initial/final setting times of slag/fly ash ratio of 70/30 mixes increase from 27/71 min to 37/85 min when the nano-silica replacement increases from 0% to 3%; while for samples with a slag/fly ash ratio of 30/70, the increment is from 76/128 min to 96/154 min. However, this result is contrary to most of the investigations about the effect of nano-silica on setting time in Portland cement systems [46–49], in which cases the nano-silica provides additional nucleation sites for the formation and growth of reaction products, so the reaction process is accelerated. Therefore, in order to have a better understanding on the role of nano-silica during the early age reaction, isothermal calorimetry tests were carried out and the results are presented in Section 3.2.

3.2. Reaction kinetics

It is generally agreed that alkali activated materials present four typical stages during the reaction process: dissolution, induction, acceleration/deceleration and stable period [50–53]. The dissolution stage usually occurs within the first few minutes after mixing and results in a significantly high heat release, which is due to the initial wetting and dissolution of raw materials. Afterwards, the newly formed reaction products cover the surface of unreacted particles and temporarily hinder the reaction process (induction period). The further reaction continues when the alkalis penetrate the covered layers and reach the raw materials again, then the second heat evolution peak that is attributed to the massive formation of reaction products appears. Finally, when the main reaction almost completes, the heat release decreases to lower levels and remains stable.

The normalized heat flow of alkali activated slag–fly ash blends (with a slag/fly ash ratio of 70/30 and nano-silica replacement from 0% to 3%) within the first 72 h are shown in Fig. 4. The heat release peaks in the dissolution stage are not shown in this figure due to their much higher magnitude. It can be seen that for samples without nano-silica addition, the heat release peak in the acceleration stage is located at around 8.3 h after mixing; while as the nano-silica content increases, this peak slightly shifts to longer times with lower intensities. For instance, when increasing the nano-silica content from 0% to 3%, the acceleration peak is slightly delayed for 0.4 h and the peak intensity decreases from 1.77 mW/g to 1.55 mW/g. Such relatively slight but detectable changes during the main reaction stage indicate that the reaction of alkali activated slag–fly ash blends is retarded to some extent in the presence of nano-silica. This phenomenon is in agreement with the setting time results in this study and confirms again the retarding effect of nano-silica on the early age reaction. Again, this result is in contrast to previous studies that the presence of nano-silica accelerates the reaction process in cement based system [49,54–56]. Then it is suggested that the isothermal calorimetry results observed in this study is a combined effect of the following factors: (1) a certain amount of nano-silica is dissolved during the early age and leads to an increment of the initial silica content in the solution, which delays the reaction of slag and fly ash. It has been known that the first step of alkali activation is the dissolution of raw materials, and during this process the Si, Ca and Al units are dissolved from the solid precursors and become available in the solution for the further reaction. Due to the fine particle size and high surface area of nano-silica, the dissolution of Si units also takes place in nano-silica particles and faster than that in slag and fly ash, which increases the initial silica content in solution and retards the dissolution of Si from slag and fly ash to some extent. Finally, the heat release peak is delayed as a result. While in cement based system, the initial pH is lower, thus the nucleation effect of nano-silica is preferred at the beginning stage instead of dissolution. (2) The addition of nano-silica accelerates the reaction process. The fine nano-silica particles that are not dissolved initially work as additional nucleation sites, which promote the formation and growth of reaction products from the dissolved units. Consequently, the reaction process is accelerated. (3) The incorporation of nano-silica leads to a decrease of effective slag content in the system, which leads to the decrease of the reaction intensity. The acceleration effect of slag on the early age reaction of blended alkali systems has been confirmed by previous studies [16,21,51]. In this case the nano-silica addition decreases the total slag content, then less presented slag (available Ca, Si units) results in a less intensive reaction process. In overall, as a final apparent result of the three influential factors analyzed above, the reaction process is slightly delayed with lower peak intensities when nano-silica is added. However, more studies are needed to be carried out in order to clarify the behavior of nano-silica in detail.

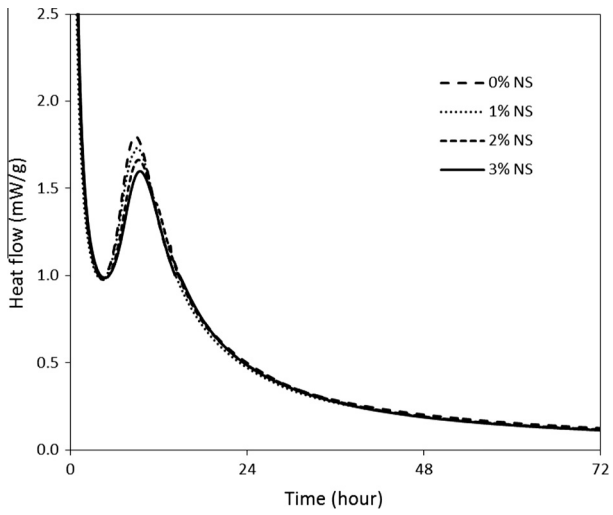

Fig. 4. Normalized heat flow of AA slag–fly ash (70/30) pastes with nano-silica addition.

Fig. 5 illustrates the normalized heat flow of samples with a slag/fly ash ratio of 30/70 and nano-silica replacement from 0% to 3%. Compared to the samples with a slag/fly ash ratio of 70/30 (see Fig. 4), it can be seen that both the induction and acceleration stages are remarkably retarded. For instance, the induction period is located at around 3.7 h in mixes with a slag/fly ash ratio of 70/30, while it delays for approximately 4.5 h when changing the slag/fly ash ratio to 30/70. Similarly, the acceleration peak shifts from about 8.3 h to 20 h, also the peak intensity decreases from about 1.5 mW/g to 0.5 mW/g. Those changes demonstrate that the slag/fly ash ratio shows a dominant influence on the early age reaction, namely increasing the slag content can effectively accelerate the main reaction stage and result in a more intensive reaction. This is due to the intrinsic differences in the amorphous structure between slag and fly ash, where slag has a higher Ca content that leads to a more disordered glassy framework than aluminosilicates dominated structure (fly ash in this case) [8], thus the slag exhibits a much higher reactivity than fly ash under alkali activation. In addition, based on the presented experimental results, it can be concluded that the early age reaction is mainly controlled by the relative slag content in the alkali activated slag–fly ash blends. Besides, similar to the results that are shown in Fig. 4, the addition of nano-silica also slightly retards the reaction and decreases the intensity of the main reaction peak, but its influence on the reaction process is relatively small compared to effect of slag content.

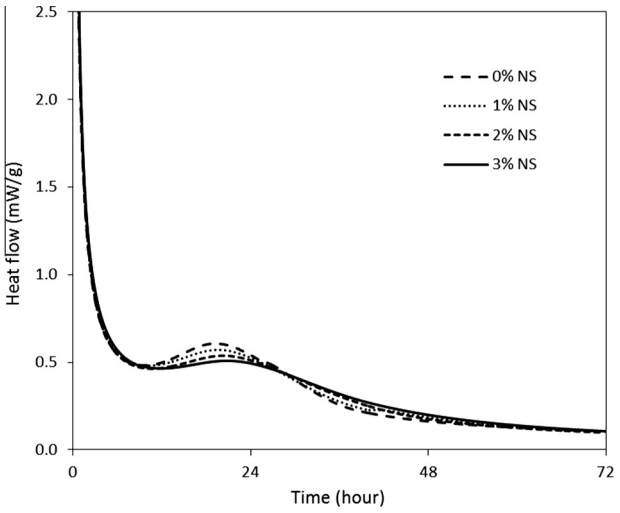

Fig. 5. Normalized heat flow of AA slag–fly ash (30/70) pastes with nano-silica addition.

3.3. FTIR analysis

Fig. 6 shows the infrared spectra of the unreacted slag, fly ash and nano-silica. It can be seen that the main vibration band for slag is located at around 900 cm^{-1}, which is assigned to the asymmetric stretching vibration of terminal Si–O bonds [57], while the main vibration band for fly ash is a bridge Si–O–T bond that is shown at around 1020 cm^{-1} [58]. The difference in the main absorption band is attributed to the structural differences in the glassy phase of raw materials. Besides, the unreacted slag shows an absorption band at around 670 cm^{-1}, which is associated with the asymmetric stretching vibration of tetrahedral T–O groups [59], while the absorption bands that are located at around 1080, and 600–800 cm^{-1} in fly ash demonstrate the presence of small amount of quartz and mullite [60]. As for the nano-silica, three main absorption bands are shown at 1100, 1640 and around 3300 cm^{-1}, respectively, indicating the presence of large amount of bridge Si–O bonds and water. It should be noted that the Si–O bond in nano-silica is located at higher wavenumbers than that in slag and fly ash, which means that the silicate in nano-silica presents a higher degree of polymerization. Small absorption bands at around 810 and 960 cm^{-1} are also shown in nano-silica, indicating that a small amount of terminal Si–O bonds is coexisting within the bridge Si–O–Si bonds.

Fig. 7 shows the infrared spectra of all mixtures after alkali activation. It can be seen that regardless of the slag/fly ash ratios and nano-silica content, all specimens exhibit absorption bands at similar location in general, demonstrating that the gel structure of ambient temperature cured alkali activated slag–fly ash blends is independent of the raw materials' composition. Specifically, all mixes show a small absorption band at around 640 cm^{-1}, which is associated with the formation vibration of TO_4 groups (where T represents Si or Al). Since this band is not observed in the starting materials, its presence may reveal that a certain amount of structural changes has occurred to the tetrahedral T–O groups during alkali activation. The vibration bands at 1640 cm^{-1} and around 3200 cm^{-1} in all samples manifest the presence of bound water within the reaction products [61]. The water observed here include both physically and chemically bound ones. It should be noted that the absorption bands at around 1420 cm^{-1}, which corresponds to the stretching vibrations of O–C–O in carbonates [19], are shown in all mixes. It seems that a certain extent of carbonation has taken place during the reaction or curing process, since the starting materials do not show the presence of C–O bonds. The carbonation behavior of the reacted gels will be analyzed in detail in the following TG/DSC analysis.

It can be seen that the main absorption band that represents the Si–O bond is shown at 950 cm^{-1} in all mixes. This band is assigned to the asymmetric stretching vibration of the non-bridging Si–O bonds [57], indicating that the reaction product is dominated by chain structured C-A-S-H gels. From the aspect of starting materials, the Si–O bond in slag is around 900 cm^{-1}; the increase in wavenumber indicates the formation of a higher polymerized Si–O network. While for the fly ash, the main absorption band shifts from 1020 cm^{-1} to lower numbers after activation, implying that the original high cross-linked bridging Si–O bonds are broken down to lower ones. Similarly, the bridge Si–O bonds in nano-silica also change to lower polymerized ones. Besides, as the nano-silica content increases from 0% to 3%, there is no remarkable change in the absorption bands of Si–O, this demonstrates that the addition of nano-silica shows negligible influences on the gel structure of alkali activated slag–fly ash blends. The fixed location of terminal Si–O bonds in the reaction products can be explained by the strong effect of calcium from slag, which hinders the influence of fly ash and nano-silica on gel structure. In the presence of slag, large amount of calcium is released at the initial stage of reaction; these divalent ions consume the available Si, Al units in the solution and prefer the formation of a less ordered structure, then considerable amount of C-A-S-H type gels with short ranged chain structure are formed as a result. In addition, the consumption of

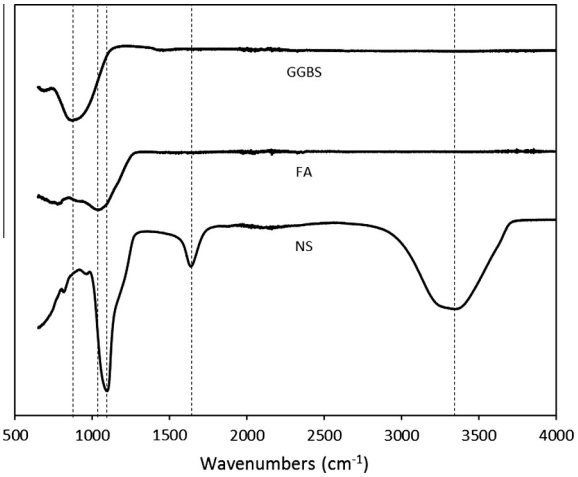

Fig. 6. FTIR spectra of the starting materials.

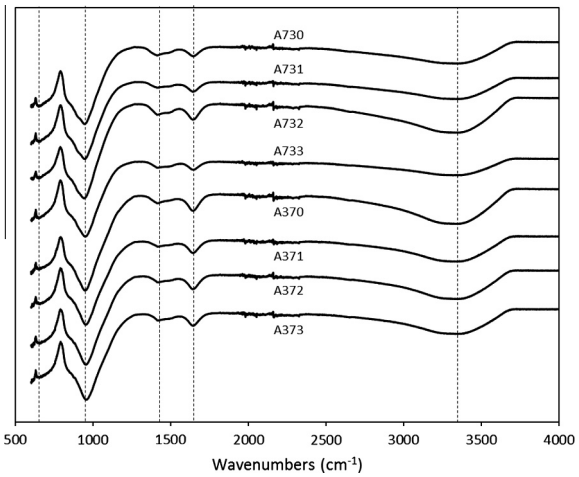

Fig. 7. FTIR spectra of AA slag–fly ash blends with nano-silica addition.

alkalis and Si, Al units limits the accumulation and polymerization process of Si, Al monomers alone, thus the silicate and alumina dominated high crosslinking networks (bridge Si–O bonds with higher wavenumbers) are not formed. On the other hand, although the addition of nano-silica increases the total available silica content to some degree, it seems that this change is not sufficient to affect the influence of calcium on gel structure.

3.4. TG/DSC analysis

The thermogravimetry results of samples with a slag/fly ash ratio of 70/30 and nano-silica additions up to 3% are presented in Fig. 8. It can be observed that all mixes exhibit a significant mass loss before around 110 °C, which is mainly due to the loss of physically bound water within the reaction products [62]. The evaporable water content is around 15.8% in all samples, indicating that the nano-silica addition has a limited effect on the physically bound water content. Afterwards, all mixtures show a negligible mass loss between 105 °C and 160 °C, followed by a gradual decrease in mass until heated to around 700 °C. The continuous mass loss after around 160 °C is assigned to the gradual decomposition of the reaction products (mainly C-A-S-H type gels), which leads to the release of chemically bound water within the generated gels. After around 700 °C, all mixes present a slight and moderate mass loss until 1000 °C; also no other abrupt mass losses are shown between 105 °C and 1000 °C. The thermogravimetry results reveal that the reaction products are mainly amorphous gels with bound water. It can be seen that as the nano-silica content increases, there is a slight but detectable increase in mass loss between 160 °C and 1000 °C. For instance, when increasing the nano-silica content from 0% to 3%, the mass loss between 160 °C and 1000 °C gradually increases from 4.69% to 5.47%. It implies that the addition of nano-silica slightly increases the amount of chemically bound water content. This is probably due to the fine particle size and high reactivity of nano-silica, which may not only work as a nucleation site, but also provide extra reactive silica source, and both effects help to bond more water within the matrix.

Fig. 9 depicts the thermogravimetry results of samples with a slag/fly ash ratio of 30/70. It is obvious that these mixes exhibit a similar mass loss procedure as the ones with the slag/fly ash ratio of 70/30. All samples show an evaporable water content of around 16.1%, which is at the same level as the ones shown in Fig. 8. Also, the mass losses between 160 °C and 1000 °C in samples without nano-silica are similar, which is 4.69% and 4.31% in samples with a slag/fly ash ratio of 70/30 and 30/70, respectively. However, there is a slight difference in the mass loss between 160 °C and around 500 °C, as can be seen that samples with a slag/fly ash ratio of 70/30 present a more abrupt decrease. Concerning the effect of nano-silica, it is clear that its beneficial effect on chemically bound water content becomes less significant. It is shown that when increasing the nano-silica content from 0% to 3%, the mass loss between 160 °C and 1000 °C is increased by 16.6% in mixes with a slag/fly ash ratio of 70/30, while this value is only 7.7% in mixes with the slag/fly ash ratio of 30/70. It is indicated that the nano-silica may increase the bound water content by mainly influencing the reaction of the calcium enriched slag, since the main reaction product is a Ca and Si dominated structure with high silicate contents; while the benefit of nano-silica may become limited when large amount of silicate is present (slag/fly ash ratio of 30/70), and its main contribution may turn into the filler effect. Nevertheless, further studies are needed in order to deeply understand the effect of nano-silica on the chemical composition of the hydrated gels in slag–fly ash blends.

Figs. 10 and 11 illustrate the differential scanning calorimetry (DSC) results of mixes with different slag/fly ash ratios and nano-silica contents. The sharp heat absorption peak that is located at around 110 °C is associated with the evaporation of the physically bound water, since a corresponding remarkable mass loss is shown at the same temperature range in the TG analysis. Afterwards, a small absorption peak at around 180 °C is observed, which is in correlation with the gradual mass loss after 105 °C in the TG results, indicating the beginning of the gradual decomposition processes of the reaction products [63]. It can be seen that when nano-silica is incorporated, all mixes feature similar locations of heat absorption peaks, which reveals again that the structure of reaction products remain the same and is independent of the nano-silica content. All mixes also show a broad and smooth heat absorption peak between 600 °C and 800 °C while without remarkable mass changes at the same temperature range. This is attributed to the decomposition of the carbonate composites that are formed due to the carbonation process during the reaction or curing stage, since no carbonate sources were added at the beginning but the O–C–O vibration bonds are observed in FTIR analysis. It seems that the carbonation behavior is not significant since the mass loss between 600 °C and 800 °C is around 0.42%, and this value may also include the mass loss of chemically bound water. It should

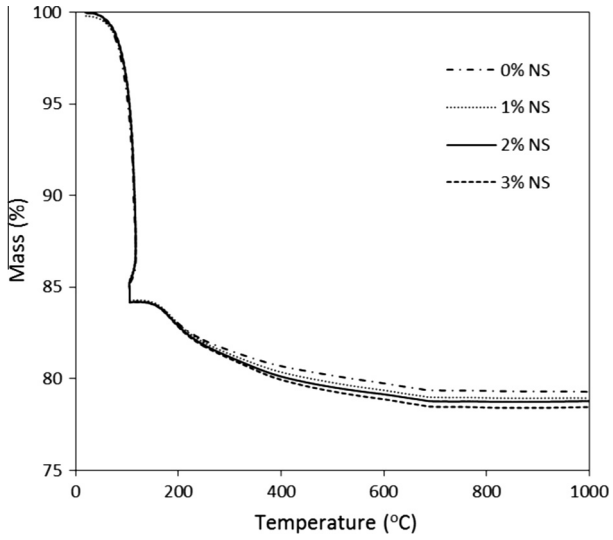

Fig. 8. TG analysis of AA slag–fly ash (70/30) pastes with nano-silica addition.

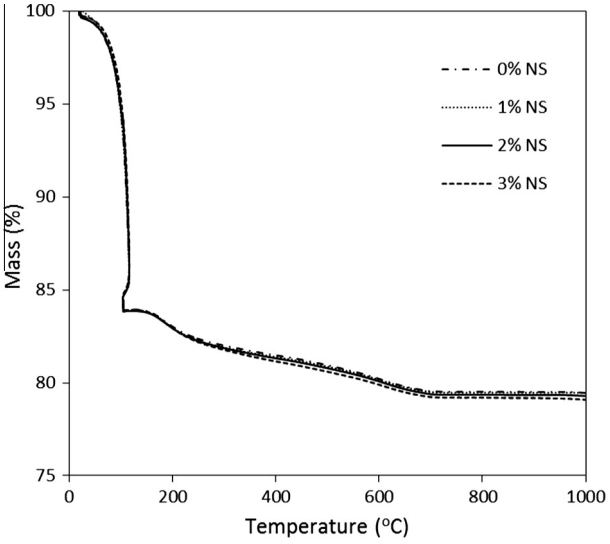

Fig. 9. TG analysis of AA slag–fly ash (30/70) pastes with nano-silica addition.

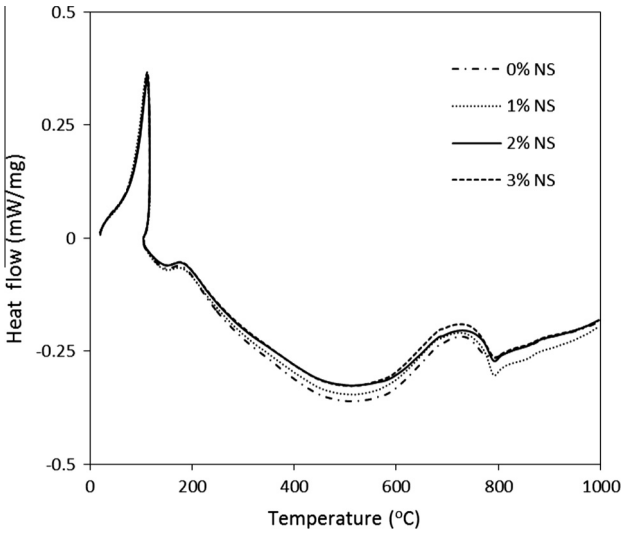

Fig. 10. DSC analysis of AA slag–fly ash (70/30) pastes with nano-silica addition.

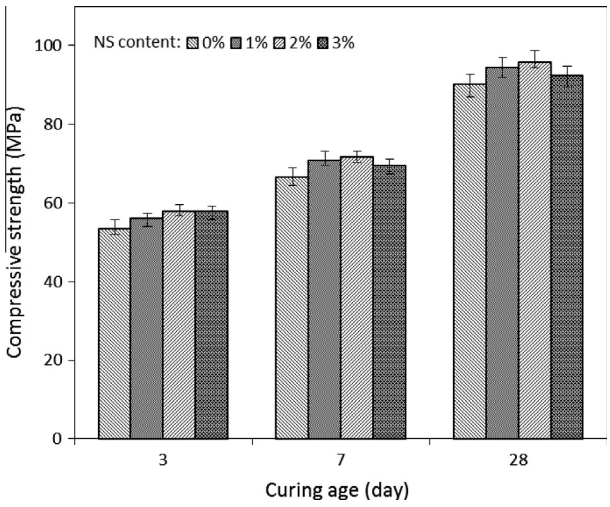

Fig. 12. Compressive strength of AA slag/fly ash blends (70/30) with nano-silica addition.

be noted that all mixtures show an exothermic peak at around 800 °C, which is attributed to the formation of crystalline phases under high temperature [63].

3.5. Compressive strength

The compressive strength of samples with a slag/fly ash ratio of 70/30 and nano-silica content from 0% to 3% is shown in Fig. 12. For mixes without nano-silica addition, the compressive strength is 53.5 MPa after 3 days of curing; and it increases to 66.6 MPa at 7 days and 90.2 MPa at 28 days. It has been known that the alkali activated slag usually exhibits relatively high strength at both early and later stages [1], and the results in this study show that satisfying strengths that are suitable for high performance applications can be obtained in ambient temperature cured slag–fly ash blends. When nano-silica is incorporated, the compressive strength is slightly increased at 3 days, and it can be seen that when increasing the nano-silica content from 0% to 3%, the compressive strength gradually increases from 53.5 MPa to 57.9 MPa. It should also be noted that when the nano-silica content reaches 2%, the strength increment is no longer significant when a higher amount of nano-silica is incorporated. Similarly, at the age of 7 days, the compressive strength is increased from 66.6 MPa to 71.6 MPa when increasing the nano-silica content up to 2%, but the strength is slightly reduced to 69.5 MPa when the nano-silica content increases to 3%. It indicates that a nano-silica content of around 2% is the optimum in terms of strength in both cases. In addition, it can be observed that the strength increasing rate is decreased as the increase of nano-silica content. For instance, the compressive strength is increased by 6.4% when increasing the nano-silica content from 0% to 1%, while this value is only 1% when the nano-silica content changes from 1% to 2%. Compared to the effect of nano-silica on strength in cement based system, the nano-silica exhibits a less significant influence in alkali activated systems [47,64,65]. One possible explanation is that in cement based system, the nano-silica not only works as a micro-filler that refines the pore structure, but also effectively consumes the calcium hydroxide which leads to the formation of extra hydrated gels; then the strength can be remarkably increased. While in alkali activated system, as can be seen from the TG/DSC analysis, no significant amount of calcium hydroxide is presented, thus the pozzolanic effect of nano-silica is limited. Therefore, the nano-silica may only benefit the compressive strength by pore refinement due to the filler effect, as well as the additional bound water due to the extra provided silica from nano-silica. Concerning the 28 days strength, when increasing the nano-silica content from 0% to 3%, the compressive strength firstly increases from 90.2 MPa to 95.9 MPa, then decreases to 92.4 MPa, showing again an optimum nano-silica content of around 2%.

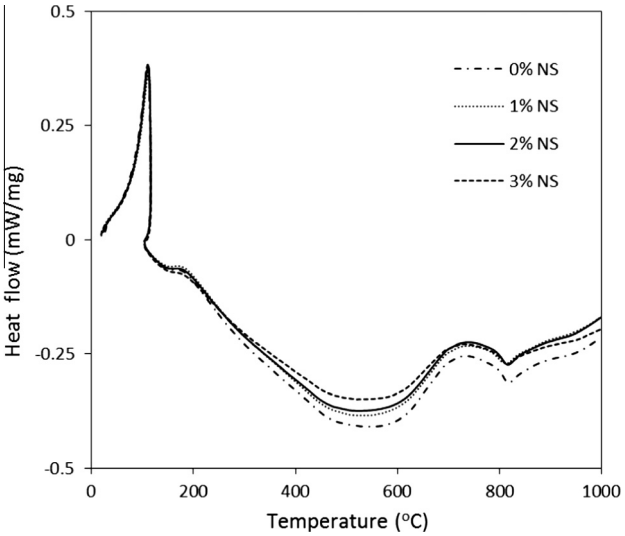

Fig. 11. DSC analysis of AA slag–fly ash (30/70) pastes with nano-silica addition.

Fig. 13 depicts the compressive strength results of samples with a slag/fly ash ratio of 30/70. It is obvious that the strength is remarkably lower than those with a slag/fly ash ratio of 70/30. This is because of the significant effect of slag content on strength, which has been well discussed in the previous studies [16,66,67]. The results shown in Figs. 12 and 13 together provide a general impression about the compressive strength ranges that are caused by solid materials' composition in alkali activated slag–fly ash blends. It can be seen that without nano-silica addition, the 3, 7 and 28 days strength are 23.6 MPa, 35.9 MPa and 54.1 MPa, respectively. The compressive is increased by 52.1% and 129% at these three typical curing ages, while in samples with a slag/fly ash ratio of 70/30, these values are 24.5% and 68.6%, indicating that there is a difference in strength development between samples with different slag/fly ash ratios. In other words samples with a higher slag

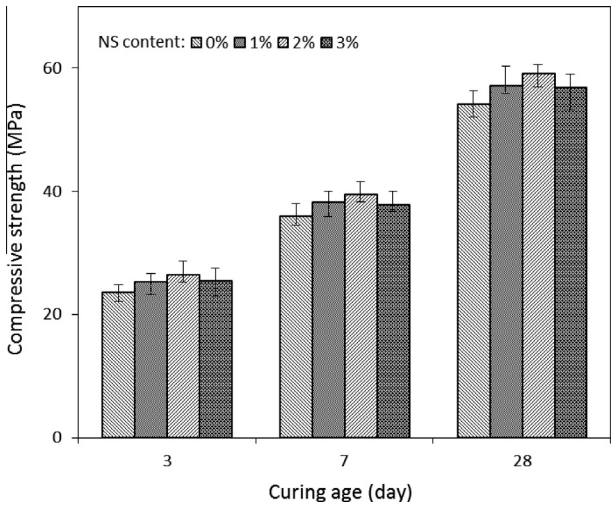

Fig. 13. Compressive strength of AA slag/fly ash blends (30/70) with nano-silica addition.

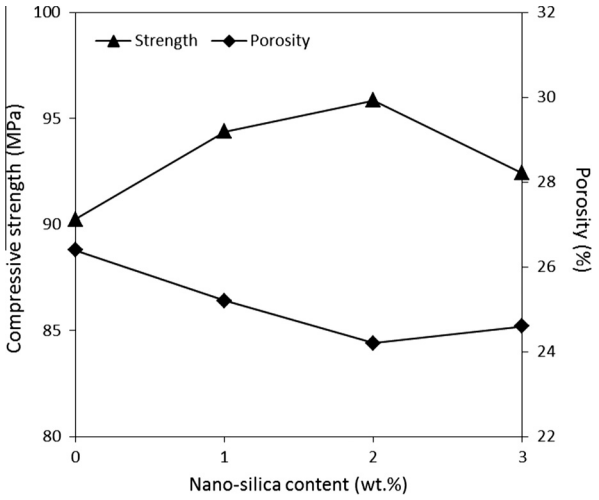

Fig. 14. Relations between 28 days strength, porosity and nano-silica content (slag/fly ash = 70/30).

content shows a higher early strength and a lower increasing rate. Similar to the results in Fig. 12, the compressive strength firstly increases when increasing the nano-silica content up to 2%, then slightly reduces when the nano-silica content reaches 3%; and this tendency becomes more significant at longer ages. The optimum nano-silica content of 2% in terms of compressive strength is shown in all mixes, and the highest strength present in samples with 2% nano-silica are 26.4 MPa at 3 days, 39.4 MPa at 7 days and 59.1 MPa at 28 days, respectively.

3.6. Water permeable porosity

Figs. 14 and 15 show the relationships between the compressive strength, nano-silica content and water permeable porosity of alkali activated slag–fly ash blends after 28 days of curing. It can be seen that the compressive strength increases with the reduction of porosity in general, which confirms again the inverse relationship between the strength and porosity in porous materials. Also, the porosity decreases with the increase of nano-silica content in general, while when increasing the nano-silica content up to 3%, the reduction of porosity becomes less significant or even slightly increases. As presented in Fig. 14, when increasing the nano-silica content from 0% to 2%, the compressive strength increases from 90.2 MPa to 95.9 MPa while the porosity decreases from 26.4% to 24.2%. However, the further increase of nano-silica content to 3% leads to a slight decrease of strength and increase of porosity. One possible explanation for this phenomenon is that a suitable content of nano-silica will refine the pore structure by filler effect and generate more reaction products; while higher contents lead to a significant reduction of workability (increased cohesiveness), as discussed in Section 3.1, which may result in an increase of the air content within the paste, then the porosity is increased as a result. Fig. 15 shows the results of samples with a slag/fly ash ratio of 30/70, it is obvious that when compared to the results shown in Fig. 14, higher porosities as well as lower compressive strengths are presented. This is due to the relatively low reactivity of fly ash under ambient temperature and its relatively high content in the slag/fly ash blends, which result in a lower content of reaction products, thus less densed matrixes and lower strengths are exhibited. Specifically, when increasing the nano-silica content from 0% to 3%, the porosity decreases from 30.5% to 27.2%, while the compressive strength firstly increases from 54.1 MPa to 59.1 MPa, then slightly decreases to 56.8 MPa at the nano-silica dosage of 3%.

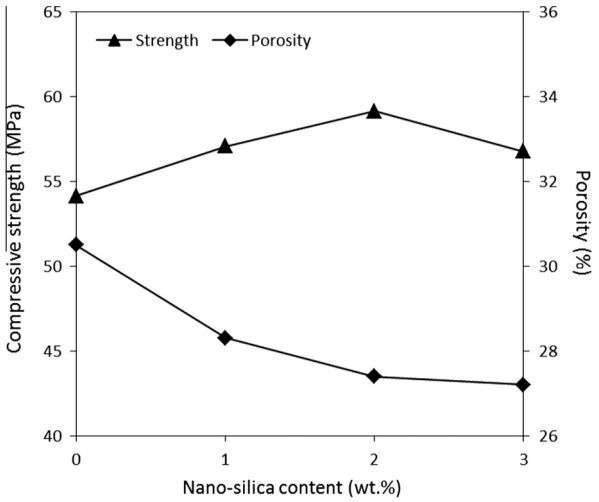

Fig. 15. Relations between 28 days strength, porosity and nano-silica content (slag/fly ash = 30/70).

4. Conclusions

This paper investigates the effects of nano-silica addition on slump flow, setting times, reaction kinetics, gel characteristics, porosity and compressive strength of alkali activated slag–fly ash blends designed with two slag/fly ash ratios; and the role of nano-silica in alkali activated system is discussed. Based on the experimental results, the following conclusions can be drawn:

- The incorporation of nano-silica significantly decreases the slump flow of paste samples due to its high surface area, also mixes with a lower slag/fly ash ratio contribute to a better flowability. Both initial and final setting times are slightly increased with the increase of nano-silica content, but slag/fly ash ratio shows a more considerable effect on setting: the higher content of slag, the faster of setting times.
- The slag content plays a dominant role during the early age reaction, since it is the main factor that affects the location and intensity of the induction and main reaction stage. The nano-silica replacement slightly retards the reaction process at early ages and also leads to a slight reduction of the peak

intensity in the main reaction stage. This phenomenon is suggested to be the synergetic effect of several factors.

- Gel character analyses conducted by FTIR and TG/DSC show that the main reaction product is a C-A-S-H type gel with chain structure, and the addition of nano-silica slightly increases the chemically bound water content. The gel structure remains stable regardless of the nano-silica content and slag/fly ash ratio.
- Higher compressive strengths are observed in samples with a higher slag content; and samples with different slag/fly ash ratios show different rates of strength development. A nano-silica addition up to around 2% benefits the compressive strength at typical curing ages of 3, 7 and 28 days, while a further higher nano-silica content shows negative effects.
- Samples with a higher slag/fly ash ratio exhibit a lower level of porosity. The porosity decreases with the increasing nano-silica content, indicating the positive effect on nano-silica on pore structure refinement. All mixes show an optimum nano-silica content of around 2% in terms of porosity reduction.

Acknowledgements

This research was supported by China Scholarship Council and the Department of the Built Environment at Eindhoven University of Technology. The authors gratefully thank Mr. P. de Vries (ENCI B. V., the Netherlands) and Mr. J. van Eijk (Knauf Insulation, the Netherlands) for the materials supply. Furthermore, the authors wish to express their gratitude to the following sponsors of the Building Materials research group at TU Eindhoven: Rijkswaterstaat Grote Projecten en Onderhoud; Graniet-Import Benelux; Kijlstra Betonmortel; Struyk Verwo; Attero; Enci; Rijkswaterstaat Zee en Delta-District Noord; Van Gansewinkel Minerals; BTE; V.d. Bosch Beton; Selor; GMB; Geochem Research; Icopal; BN International; Eltomation; Knauf Gips; Hess AAC Systems; Kronos; Joma; CRH Europe Sustainable Concrete Centre; Cement & Beton Centrum; Heros and Inashco (in chronological order of joining).

References

[1] S.D. Wang, K.L. Scrivener, P.L. Pratt, Factors affecting the strength of alkali-activated slag, Cem. Concr. Res. 24 (6) (1994) 1033–1043.
[2] A. Fernández-Jiménez, I. García-Lodeiro, A. Palomo, Durable characteristics of alkali activated fly ashes, J. Mater. Sci. 42 (2007) 3055–3065.
[3] T. Bakharev, J.G. Sanjayan, Y.B. Cheng, Resistance of alkali-activated slag concrete to acid attack, Cem. Concr. Res. 33 (2003) 1607–1611.
[4] Y.Z. Hai, K. Venkatesh, L.Q. Shu, C. Liang, W. Bo, Development of metakaolin–fly ash based geopolymers for fire resistance applications, Constr. Build. Mater. 55 (2014) 38–45.
[5] A.M. Rashad, A comprehensive overview about the influence of different additives on the properties of alkali-activated slag – a guide for Civil Engineer, Constr. Build. Mater. 47 (2013) 29–55.
[6] C.J. Shi, A. Fernández Jiménez, A. Palomo, New cements for the 21st century: the pursuit of an alternative to Portland cement, Cem. Concr. Res. 41 (2011) 750–763.
[7] A.R. Brough, A. Atkinson, Sodium silicate-based alkali-activated slag mortars: Part I. Strength, hydration and microstructure, Cem. Concr. Res. 32 (2002) 865–879.
[8] Li. Chao, Sun. Henghu, Li. Longtu, A review: the comparison between alkali-activated slag (Si + Ca) and metakaolin (Si + Al) cements, Cem. Concr. Res. 40 (2010) 1341–1349.
[9] N.K. Lee, H.K. Lee, Setting and mechanical properties of alkali-activated fly ash/slag concrete manufactured at room temperature, Constr. Build. Mater. 47 (2013) 1201–1209.
[10] M. Rashad Alaa, Properties of alkali-activated fly ash concrete blended with slag, Iran. J. Mater. Sci. Eng. 10 (1) (2013) 57–64.
[11] S. Aydin, A ternary optimization of mineral additives of alkali activated cement mortars, Constr. Build. Mater. 43 (2013) 131–138.
[12] T. Sugama, L.E. Brothers, T.R. Van de Putte, Acid-resistant cements for geothermal wells: sodium silicate activated slag/fly ash blends, Adv. Cem. Res. 17 (2) (2005) 65–75.
[13] C.K. Yip, G.C. Lukey, J.S.J. van Deventer, The coexistence of geopolymeric gel and calcium silicate hydrate at the early stage of alkaline activation, Cem. Concr. Res. 35 (2005) 1688–1697.
[14] I. García-Lodeiro, D.E. Macphee, A. Palomo, A. Fernández-Jiménez, Effect on fresh C-S-H gels the simultaneous addition of alkali and aluminium, Cem. Concr. Res. 40 (2010) 27–32.
[15] I. Ismail, S.A. Bernal, J.L. Provis, R.S. Nicolas, S. Hamdan, J.S.J. Deventer, Modification of phase evolution in alkali-activated blast furnace slag by the incorporation of fly ash, Cem. Concr. Compos. 45 (2014) 125–135.
[16] S. Kumar, R. Kumar, S.P. Mehrotra, Influence of granulated blast furnace slag on the reaction, structure and properties of fly ash based geopolymer, J. Mater. Sci. 45 (3) (2010) 607–615.
[17] M. Chi, R. Huang, Binding mechanism and properties of alkali-activated fly ash/slag mortars, Constr. Build. Mater. 40 (2013) 291–298.
[18] F. Puertas, S. Martínez-Ramírez, S. Alonso, E. Vázquez, Alkali-activated fly ash/slag cement. Strength behaviour and hydration products, Cem. Concr. Res. 30 (2000) 1625–1632.
[19] S.A. Bernal, J.L. Provis, V. Rose, A. Mejía de Gutierrez, Evolution of binder structure in sodium silicate-activated slag–metakaolin blends, Cem. Concr. Compos. 33 (2011) 46–54.
[20] S.A. Bernal, A. Mejía de Gutierrez, J.L. Provis, Engineering and durability properties of concretes based on alkali-activated granulated blast furnace slag/metakaolin blends, Constr. Build. Mater. 33 (2012) 99–108.
[21] X. Gao, Q.L. Yu, H.J.H. Brouwers, Reaction kinetics, gel character and strength of ambient temperature cured alkali activated slag–fly ash blends, Constr. Build. Mater. 80 (2015) 105–115.
[22] F. Pacheco-Torgal, S. Miraldo, Y. Ding, J.A. Labrincha, Targeting HPC with the help of nanoparticles: an overview, Constr. Build. Mater. 38 (2013) 365–367.
[23] F.U.A. Shaikh, S.W.M. Supit, P.K. Sarker, A study on the effect of nano silica on compressive strength of high volume fly ash mortars and concretes, Mater. Des. 60 (2014) 433–442.
[24] A. Said, M. Zeidan, M. Bassuoni, Y. Tian, Properties of concrete incorporating nano-silica, Constr. Build. Mater. 36 (2012) 838–844.
[25] M.H. Zhang, H. Li, Pore structure and chloride permeability of concrete containing nano-particles for pavement, Constr. Build. Mater. 25 (2011) 608–616.
[26] J.Y. Shih, T.P. Chang, T.C. Hsiao, Effect of nanosilica on characterization of Portland cement composite, Mater. Sci. Eng., A 424 (2006) 266–274.
[27] J. Björnström, A. Martinelli, A. Matic, L. Börjesson, I. Panas, Accelerating effects of colloidal nano-silica for beneficial calcium-silicate-hydrate formation in cement, Chem. Phys. Lett. 392 (2004) 242–248.
[28] Y. Qing, Z. Zenan, K. Deyu, C. Rongshen, Influence of nano-SiO_2 addition on properties of hardened cement paste as compared with silica fume, Constr. Build. Mater. 21 (2007) 539–545.
[29] K.L. Lin, W.C. Chang, D.F. Lin, H.L. Luo, M.C. Tsai, Effects of nano-SiO_2 and different ash particle sizes on sludge ash–cement mortar, J. Environ. Manage. 88 (2008) 708–714.
[30] J.J. Gaitero, I. Campillo, A. Guerrero, Reduction of the calcium leaching rate of cement paste by addition of silica nanoparticles, Cem. Concr. Res. 38 (2008) 1112–1118.
[31] M. Schmidt, K. Amrhein, T. Braun, C. Glotzbach, S. Kamaruddin, R. Tanzer, Nanotechnological improvement of structural materials – impact on material performance and structural design, Cem. Concr. Compos. 36 (2013) 3–7.
[32] T. Phoo-ngernkham, P. Chindaprasirt, V. Sata, S. Hanjitsuwan, S. Hatanaka, The effect of adding nano-SiO_2 and nano-Al_2O_3 on properties of high calcium fly ash geopolymer cured at ambient temperature, Mater. Des. 55 (2014) 58–65.
[33] K. Gao, K.L. Lin, D.Y. Wang, C.L. Hwang, B.L. Anh Tuan, H.S. Shiu, T.W. Cheng, Effect of nano-SiO_2 on the alkali-activated characteristics of metakaolin-based geopolymers, Constr. Build. Mater. 48 (2013) 441–447.
[34] D. Adak, M. Sarkar, S. Mandal, Effect of nano-silica on strength and durability of fly ash based geopolymer mortar, Constr. Build. Mater. 70 (2014) 453–459.
[35] X. Gao, Q.L. Yu, H.J.H. Brouwers, Properties of alkali activated slag–fly ash blends with limestone addition, Cem. Concr. Compos. 59 (2015) 119–128.
[36] British standard EN 1015-3:1999. Methods of test for mortar for masonry Part 3: Determination of consistence of fresh mortar.
[37] British standard EN 196-3:2005. Methods of testing cement Part 3: Determination of setting times and soundness.
[38] British standard EN 196-1:2005. Methods of testing cement Part 1: Determination of strength.
[39] NT Build 492. Concrete, mortar and cement-based repair materials: chloride migration coefficient from non-steady-state migration experiments.
[40] K.H. Yang, J.K. Song, K.S. Lee, A.F. Ashrour, Flow and compressive strength of alkali-activated mortars, ACI Mater. J. 106 (2009) 50–58.
[41] K.H. Yang, J.K. Song, A.F. Ashour, E.T. Lee, Properties of cementless mortars activated by sodium silicate, Constr. Build. Mater. 22 (2008) 1981–1989.
[42] B.B. Mukharjee, S.V. Barai, Assessment of the influence of nano-silica on the behavior of mortar using factorial design of experiments, Constr. Build. Mater. 68 (2014) 416–425.
[43] A. Boshehrian, P. Hosseini, Effect of nano-SiO_2 particles on properties of cement mortar applicable for ferrocement elements, Concr. Res. Lett. 2 (1) (2011) 167–180.
[44] I. Ismail, S.A. Bernal, J.L. Provis, S. Hamdan, J.S.J. van Deventer, Microstructural changes in alkali activated fly ash/slag geopolymers with sulfate exposure, Mater. Struct. 46 (3) (2013) 361–373.
[45] J.G. Jang, N.K. Lee, H.K. Lee, Fresh and hardened properties of alkali-activated fly ash/slag pastes with superplasticizers, Constr. Build. Mater. 50 (2014) 169–176.
[46] S. Luciano, L. Joao, V.M. Ferreira, H. Dachmir, R. Wellington, Effect of nano-silica on rheology and fresh properties of cement pastes and mortars, Constr. Build. Mater. 23 (2009) 2487–2491.

[47] Q. Ye, Z.A. Zhang, D.Y. Kong, R.S. Chen, Influence of nano-SiO_2 addition on properties of hardened cement paste as compared with silica fume, Constr. Build. Mater. 21 (2007) 539–545.
[48] M.H. Zhang, J. Islam, S. Peethamparan, Use of nano-silica to increase early strength and reduce setting time of concretes with high volumes of slag, Cem. Concr. Compos. 34 (2012) 650–662.
[49] P.K. Hou, S. Kawashima, K.J. Wang, D.J. Corr, J.S. Qian, S.P. Shah, Effects of colloidal nanosilica on rheological and mechanical properties of fly ash-cement mortar, Cem. Concr. Compos. 35 (2013) 12–22.
[50] E. Deira, B.S. Gebregziabiher, S. Peethamparan, Influence of starting material on the early age hydration kinetics, microstructure and composition of binding gel in alkali activated binder systems, Cem. Concr. Compos. 48 (2014) 108–117.
[51] S. Chithiraputhiran, N. Neithalath, Isothermal reaction kinetics and temperature dependence of alkali activation of slag, fly ash and their blends, Constr. Build. Mater. 45 (2013) 233–242.
[52] C. Shi, R.L. Day, A calorimetric study of early hydration of alkali-slag cements, Cem. Concr. Res. 25 (1995) 1333–1346.
[53] S. Song, H.M. Jennings, Pore solution chemistry of alkali-activated ground granulated blast-furnace slag, Cem. Concr. Res. 29 (1999) 159–170.
[54] B.W. Jo, C.H. Kim, G.H. Tae, J.B. Park, Characteristics of cement mortar with nano-SiO_2 particles, Constr. Build. Mater. 21 (2007) 1351–1355.
[55] G. Land, D. Stephan, The influence of nano-silica on the hydration of ordinary Portland cement, J. Mater. Sci. 47 (2012) 1011–1017.
[56] A. Nazari, S. Riahi, The effects of SiO_2 nanoparticles on physical and mechanical properties of high strength compacting concrete, Compos. B 42 (2011) 570–578.
[57] Z.H. Zhang, H. Wang, J.L. Provis, F. Bullen, A. Reid, Y.C. Zhu, Quantitative kinetic and structural analysis of geopolymers. Part 1. The activation of metakaolin with sodium hydroxide, Thermochim. Acta 539 (2012) 23–33.
[58] A. Hajimohammadi, J.L. Provis, J.S.J. Deventer, Time-resolved and spatially resolved infrared spectroscopic observation of seeded nucleation controlling geopolymer gel formation, J. Colloid Interface Sci. 357 (2011) 384–392.
[59] G. Kovalchuk, A. Fernandez-Jimenez, A. Palomo, Alkali-activated fly ash: effect of thermal curing conditions on mechanical and microstructural development – Part II, Fuel 86 (2007) 315–322.
[60] M. Criado, A. Fernandez-Jimenez, A. Palomo, Alkali activation of fly ash: effect of the SiO_2/Na_2O ratio Part I: FTIR study, Microporous Mesoporous Mater. 106 (2007) 180–191.
[61] P. Yu, R.J. Kirkpatrick, B. Poe, P.F. McMillan, X. Cong, Structure of calcium silicate hydrate (C-S-H): near-, mid-, and far-infrared spectroscopy, J. Am. Ceram. Soc. 82 (3) (1999) 742–748.
[62] D.L.Y. Kong, J.G. Sanjayan, Effect of elevated temperatures on geopolymer paste, mortar and concrete, Cem. Concr. Res. 40 (2010) 334–339.
[63] P. Rovnaník, P. Bayer, P. Rovnaníková, Characterization of alkali activated slag paste after exposure to high temperatures, Constr. Build. Mater. 47 (2013) 1479–1487.
[64] Q. Ye, Z.N. Zhang, L. Sheng, R.S. Chen, A comparative study on the pozzolanic activity between nano-SiO_2 and silica fume, J. Wuhan Univ. Technol. – Mater. Sci. Ed. 21 (3) (2006) 153–157.
[65] W.T. Kuo, K.L. Lin, W.C. Chang, H.L. Luo, Effects of nano materials on properties of waterworks sludge ash cement paste, J. Ind. Eng. Chem. 12 (5) (2006) 702–709.
[66] J.I. Escalante García, K. Campos-Venegas, A. Gorokhovsky, A. Fernández, Cementitious composites of pulverised fuel ash and blast furnace slag activated by sodium silicate: effect of Na_2O concentration and modulus, Adv. Appl. Ceram. 105 (4) (2006) 201–208.
[67] W.G. Shen, Y.H. Wang, T. Zhang, M.K. Zhou, J.S. Li, X.Y. Cui, Magnesia modification of alkali-activated slag fly ash cement, J. Wuhan Univ. Technol. – Mater. Sci. Ed. 26 (2011) 121–125.